Optofluidic wavelength division multiplexing for single-virus detection

Damla Ozcelik[a,1], Joshua W. Parks[a,1], Thomas A. Wall[b], Matthew A. Stott[b], Hong Cai[a], Joseph W. Parks[c], Aaron R. Hawkins[b], and Holger Schmidt[a,2]

[a]Department of Electrical Engineering, University of California, Santa Cruz, CA 95064; [b]Department of Electrical and Computer Engineering, Brigham Young University, Provo, UT 84602; and [c]Department of Chemistry and Biochemistry, University of California, Santa Cruz, CA 95064

Edited by David A. Weitz, Harvard University, Cambridge, MA, and approved September 16, 2015 (received for review June 17, 2015)

Optical waveguides simultaneously transport light at different colors, forming the basis of fiber-optic telecommunication networks that shuttle data in dozens of spectrally separated channels. Here, we reimagine this wavelength division multiplexing (WDM) paradigm in a novel context—the differentiated detection and identification of single influenza viruses on a chip. We use a single multimode interference (MMI) waveguide to create wavelength-dependent spot patterns across the entire visible spectrum and enable multiplexed single biomolecule detection on an optofluidic chip. Each target is identified by its time-dependent fluorescence signal without the need for spectral demultiplexing upon detection. We demonstrate detection of individual fluorescently labeled virus particles of three influenza A subtypes in two implementations: labeling of each virus using three different colors and two-color combinatorial labeling. By extending combinatorial multiplexing to three or more colors, MMI-based WDM provides the multiplexing power required for differentiated clinical tests and the growing field of personalized medicine.

integrated optics | optofluidics | single-virus detection | biosensing | multimode interferometer

The ability to overlay multiple electromagnetic waves in the same physical space by virtue of linear superposition is arguably at the root of modern communication as we know it. Originally implemented in the radiofrequency regime, this wavelength division multiplexing (WDM) principle was transferred to optical wavelengths in the visible and near-infrared range, which can be carried by a single, low-loss silica fiber (1). Available in both coarse and dense varieties, terabits of data are now shuttled between a source and their destination using anywhere from 4 to over 100 wavelengths (2, 3). Here, we transfer the WDM principle from data communications into a different realm, that of chip-based biomedical analysis, where much can be gained by superimposing multiple colors in an optical waveguide, albeit for different reasons.

First, one of the key requirements for diagnostic test panels, aside from high sensitivity and specificity, is the ability to multiplex, i.e., detect and identify multiple biomarkers simultaneously. A standard influenza test, for example, simultaneously screens for eight pathogen types, enabling differential diagnosis of diseases with similar early symptoms (www.questdiagnostics.com/testcenter/testguide.action?dc=TS_RespVirusPanel). Current gold-standard techniques for nucleic acid and protein detection such as PCR and ELISA use fluorescent organic dyes as a means of signal reporting (4). Optical detection, by fluorescence or "label-free," is extremely sensitive, allowing for single-molecule and even single-dye detection under appropriate conditions (5–11). The availability of over a dozen dyes across the visible spectrum opens the door to implementing the desired multiplexing capability with multiple dyes, i.e., spectral channels (12–14). Secondly, diagnostic tests are rapidly transitioning toward integrated laboratory-on-chip platforms on which small volumes of biological or chemical samples can be rapidly analyzed. The WDM principle of routing all spectral channels through the same physical space is, therefore, ideal for increasing compactness of an analytic device. Finally, chip-scale integration has recently been advanced by the advent of optofluidic devices in which both fluidic and optical components are miniaturized in the same system (15–17).

Here, we implement WDM on an optofluidic platform for on-chip analysis of single influenza viruses. In place of silica fiber as the physical carrier, we create a single waveguide structure that combines multiple spectral channels for fluorescence excitation of biological targets. Instead of temporally modulating each channel to transport information, we use this waveguide to produce wavelength-dependent spatial patterns in an intersecting fluidic channel. The spatial encoding of spectral information then allows for direct identification of multiple labeled targets with extremely high sensitivity and fidelity. The technique is demonstrated in two implementations for direct counting and identification of individual virus particles from three different influenza A subtypes—H1N1, H2N2, and H3N2—at clinically relevant concentrations.

Results

Optofluidic WDM with MMI Waveguide. Fig. 1*A* schematically shows the principle of WDM fluorescence detection on an optofluidic chip. A wide solid-core optical waveguide acts as an MMI waveguide in which numerous waveguide modes with different propagation constants interfere as they propagate along the structure (18). At propagation distances where the relative phases of these modes match up correctly, well-defined images (spot patterns), including self-images of the original input mode, are created. Here, we design the MMI such that a fluidic microchannel intersects the waveguide at a position that corresponds to a well-defined, integer number of spots for multiple wavelengths. Fig. 1*A* shows the

Significance

The ability to simultaneously detect and identify multiple biological particles or biomarkers is one of the key requirements for molecular diagnostic tests that are becoming even more important as personalized and precision medicine place increased emphasis on such capabilities. Integrated optofluidic platforms can help create such highly sensitive, multiplexed assays on a small, dedicated chip. We introduce a method for multiplex fluorescence detection of single bioparticles by creating color-dependent excitation spot patterns from a single integrated waveguide structure. Detection and identification of individual virus particles from three different influenza subtypes are demonstrated. The principle can be readily applied to amplification-free detection of nucleic acid biomarkers as well as larger target numbers using combinatorial color coding.

Author contributions: A.R.H. and H.S. designed research; D.O., Joshua W. Parks, T.A.W., M.A.S., and H.C. performed research; Joseph W. Parks contributed new reagents/analytic tools; D.O., Joshua W. Parks, H.C., A.R.H., and H.S. analyzed data; and D.O., Joshua W. Parks, A.R.H., and H.S. wrote the paper.

The authors declare no conflict of interest.

This article is a PNAS Direct Submission.

[1]D.O. and Joshua W. Parks contributed equally to this work.

[2]To whom correspondence should be addressed. Email: hschmidt@soe.ucsc.edu.

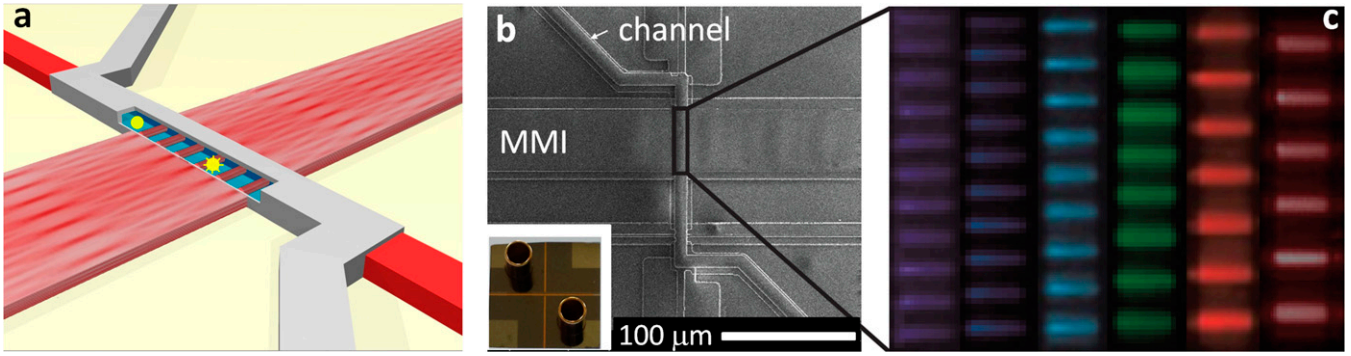

Fig. 1. WDM for single-virus detection. (*A*) Schematic view of MMI waveguide intersecting a fluidic microchannel containing target particles. Targets are optically excited as they flow past well-defined excitation spots created by the MMI; fluorescence is collected by the liquid-core waveguide channel and routed into solid-core waveguides (red). (*B*) Scanning electron micrograph of MMI-based optofluidic chip. (*Inset*) Photograph of 1-cm by 1-cm chip, showing two fluidic reservoirs holding microliters of sample volume. (C) Photographs of multispot excitation patterns created in fluidic channel filled with fluorescent liquid. The entire visible spectrum is covered by independent channels (405 nm/11 spots, 453/10, 488/9, 553/8, 633/7, 745/6). (The original black and white color scale was rendered in the actual excitation colors.)

example of six spots for excitation in the dark red (745-nm) spectral range. A particle labeled for excitation at this wavelength creates six signal emission peaks that are equally spaced in time as it flows through the channel at constant speed. Emitted photons are captured and routed to a detector if the channel also acts as a liquid-core optical waveguide (19–22). This type of multispot excitation can be used to significantly enhance the signal-to-noise ratio of a fluorescence assay (13, 23). The SEM image in Fig. 1*B* shows the physical implementation of this concept—an optofluidic platform that combines solid-core and liquid-core antiresonant reflecting optical waveguides (ARROWs). The full chip, including fluidic reservoirs for introducing microliters of sample volume into the channel, is shown in Fig. 1*B* (*Inset*). Using single-mode waveguides, this platform has demonstrated single-particle fluorescence detection sensitivity, e.g., for viruses (19) and nucleic acids (20).

The true power of the MMI approach, however, is to leverage the large available spectral bandwidth in a single photonic structure. This is evident if we consider that the product of spot number N and wavelength λ for a specific MMI can be derived from standard MMI theory (18), given by

$$N \cdot \lambda = \frac{n_C w^2}{L}, \qquad [1]$$

where w is the effective MMI width (here, 100 μm), n_c the effective refractive index of the MMI (here, 1.46), and L the MMI length (here, 3.4 mm). This allows us to implement on-chip WDM by creating physically different excitation patterns simultaneously from a single MMI. For the device used in this study, we were able to produce six well-defined spot patterns across the visible spectrum using wavelengths ranging from 405 nm (11 spots) to 745 nm (6 spots). Fig. 1*C* shows all of the excitation patterns created when the intersecting fluidic channel was filled with solutions containing fluorescent liquid (a seventh channel at 886 nm with five spots was also observed). The number and spectral positions of these six channels are a perfect match to the absorption spectra of commercially available fluorescent dyes (12). The differences in spot number and spacing are evident and constitute the basis for a new multiplex pathogen analysis technique. This multiplexing capability is ultimately limited by the finite absorption bandwidth of the dye labels which can lead to channel cross-talk if the absorption spectra overlap. However, six to seven channels can be used with proper design, enabling detection of dozens of targets using the combinatorial technique described below.

Multiplexed Single-Virus Detection with Single-Color Labeling. For the virus detection assays, three deactivated virus types were labeled with one or two of the selected fluorescent dyes (for details see *Methods*) and up to three of the channels shown in Fig. 1*C* were used. The viruses were mixed and a 5-μL aliquot was pipetted into one of the reservoirs covering the ends of the fluidic channel (Fig. 1*B*, *Inset*). The solution was then pulled through the channel and past the MMI excitation areas using negative pressure applied to the second reservoir. Light from up to three lasers was coupled into single-mode optical fiber and into a single-mode solid-core waveguide connecting the MMI to the edge of the chip. The excitation wavelengths (488, 633, and 745 nm) were chosen to create nine, seven, and six spots, respectively (Fig. 1*C*).

We implemented two multiplex assays and analyzed them with two different methods to demonstrate the capabilities of our approach. For the first assay, each of the three virus types was labeled with a different dye and all three excitation wavelengths were used.

Fig. 2*A* shows a representative fluorescence signal $F(t)$ emitted from a single H1N1 virus at 488-nm excitation, collected along the liquid-core waveguide channel. Nine distinct peaks are clearly visible, illustrating both the high quality of the MMI pattern and the sensitivity of the optofluidic chip to single-virus particles using only waveguides for excitation and collection. The virus type can be identified visually by the number of peaks (here, nine), but more sophisticated analysis algorithms can be applied that are compatible with rapid and automated signal processing of large numbers of particles in a clinical setting. For this assay, we used single-particle autocorrelations for demultiplexing. A virus particle can be detected if its fluorescence intensity exceeds the maximum background level. This background is due to residual photoluminescence of the solid waveguide materials, which was minimized by the choice of cladding materials (*Methods*). We then set a threshold level at and above which particles are analyzed to identify the subtype. This is done by performing an autocorrelation on the single multipeak signal. The detection threshold was set to 11 cts/0.1ms to ensure high confidence identification without false positives. Fig. 2*B* shows the autocorrelation signal $G(\tau)$ corresponding to the event of Fig. 2*A*. As is typical for fluorescence correlation spectroscopy, a curve with an overall decay due to drift and diffusion is observed (dashed line) (24). Superimposed on this, however, we observe a number of distinct peaks that arise at integer multiples of the lag time Δt that correspond to the time it takes the particle to travel between excitation spots. Fig. 2*C* shows close-ups of the autocorrelations for each virus type in the region of these cross-correlation peaks. The drift-induced overall decay seen in Fig. 2*B* was subtracted from each trace. Corresponding peaks are clearly separated

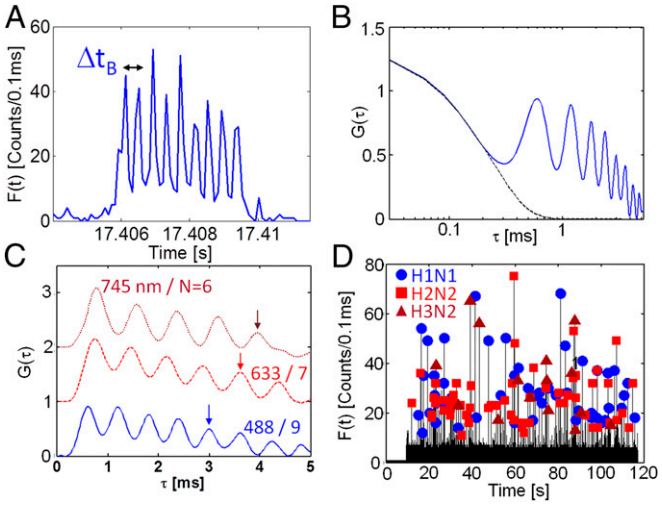

Fig. 2. Three-color multiplex virus detection. (*A*) Representative fluorescence signal emitted by single H1N1 virus excited at 488 nm showing nine distinct peaks spaced by Δt_B. (*B*) Corresponding single-particle autocorrelation signal. Multiple peaks are observed at multiples of Δt_B; dashed line: fit to underlying flow-limited correlations. (*C*) Single-particle autocorrelation for three virus types after subtraction of flow-based contribution. The peak positions depend strongly on excitation spot number (arrows mark the fifth peak for each virus type). (*D*) Segment of fluorescence from virus mixture excited at all three colors. Events are identified using single-particle autocorrelations. All but one identified signals (99.2%) agree with manual inspection of events.

(see arrows for fifth peak) and allow for correct assignment of the virus. By using the delay time for the fifth peaks, we analyzed the fluorescence trace from a particle mixture over 120 s as shown in Fig. 2*D*. Note that neither spectral separation nor filtering of the emitted light was needed. All spectral information was extracted from the temporally encoded detector signal. The symbols in Fig. 2*D* indicate the virus type identified using single-particle autocorrelations. All but one event (0.8% false positive rate) were correctly assigned as verified by manual inspection of each signal for peak number and spacing. Seventy-three events had peak intensities between the maximum background level and our threshold and were not assigned to a subtype (false negatives). We note that the individual fluorescence signal intensities vary in the form of a Poisson distribution due to differences in the position of the particles within the waveguide cross-section (20). This produces variations in the excitation and collection efficiencies in accordance with the optical mode profiles in the solid-core excitation and liquid-core collection waveguide (20). Here, (15 ± 2)% of all particles have peak intensities below the maximum background signal and are not detected, representing a false negative baseline. The virus concentrations were measured from the count rates and flow speed (H1N1, 3.2×10^6/mL; H2N2, 2.0×10^6/mL; H3N2, 8.9×10^5/mL). This shows that we were able to carry out high-fidelity multiplex detection of single viruses at clinically relevant concentrations (25–28). For the MMI used here (illuminated volume: 5 μm × 12 μm × 100 μm = 6 pL), limitations due to simultaneous presence of multiple targets in the excitation volume do not arise until concentrations exceed 1.67×10^8/mL—well above the viral titer range of influenza and other diseases (25–28).

Multiplexed Single-Virus Detection with Combinatorial Labeling. For some applications 3× multiplexing is already sufficient, but extended differentiation is often desired. Simply increasing the number of wavelengths quickly reaches a limit due to limited choice of fluorescent dyes and laser sources as well as overlapping emission spectra. A combinatorial approach, however, which assigns multiple labels to a target, can be scaled up favorably. Here, we demonstrate combinatorial multiplexing with MMI excitation using two colors for identifying three virus types. To this end, H1N1 (blue) and H3N2 (dark red) remained singly labeled (see Fig. 3*A*) whereas the H2N2 virus was colabeled with both blue and dark red dye (see Fig. 4*A*). Again, we analyzed a mixture of all three viruses, now simultaneously excited by two sources. We implemented a different signal-processing algorithm to demultiplex the virus types. Fig. 3*B* shows the fluorescence signal $F(t)$ from a single H3N2 virus. $F(t)$ is shifted and multiplied with itself $N-1$ times to create a processed signal

$$S(t,\Delta t) = \prod_{i=0}^{N-1} F(t - i \cdot \Delta t). \qquad [2]$$

$S(t,\Delta t)$ will take on a large value only at the correct Δt value(s) for a given signal, allowing us to define two color channels when Eq. **2** is applied with Δt_B and Δt_{DR}, respectively. This shift-multiply algorithm also increases the signal-to-noise ratio (SNR) of the particle detection (23). This SNR improvement is evident in Fig. 3*C*, which shows $S(t,\Delta t)$ for the mixed signal of Fig. 3*B* at Δt_{DR} = 0.63 ms (dark red).

Fig. 4*A* shows the labeling and individual fluorescence signals for all three virus types under two-color excitation. Most notably, the signal for the double-labeled H2N2 changes and clearly shows a superposition of the nine-spot (488-nm) and six-spot (745-nm) patterns. For further analysis, we first identified the average shift times Δt_B and Δt_{DR} for blue and dark red excitation using single-color excitation. Then, each event of the mixed assay was analyzed using Eq. **2** at those Δt values. Fig. 4*B* shows that a blue-labeled H1N1 virus only shows appreciable $S(t)$ at Δt_B. Likewise, an H3N2 virus shows strong signal in the Δt_{DR} channel. The double-labeled virus, however, shows large $S(t)$ in both channels, demonstrating that we can successfully identify three different viruses with two colors.

Discussion

If we only rely on unique combinations of three colors, we can distinguish seven targets. With four colors, 15× spectral multiplexing is possible, sufficient for the vast majority of diagnostic panels. The readout fidelity depends on the ratio of spot spacing (determined by the MMI width w) and the individual spot width (determined by the width of the input single-mode waveguide w_i) and can be further improved by increasing w/w_i. Moreover, multiple fluidic channels addressed with MMIs of different dimensions can further increase the multiplexing power. The multicolor labeling strategy can readily be extended to fluorescently labeled nucleic acids and antibodies specific to target surface proteins. The planar optical architecture also allows for further integration of a dedicated microfluidic layer for upstream sample processing and distribution (29–31) as well as techniques for focusing the particles in the center of the fluidic channel (32) for optimized detection efficiency.

MMI-based WDM is clearly ideal for on-chip bioanalysis, providing the missing element to turn an optofluidic chip with

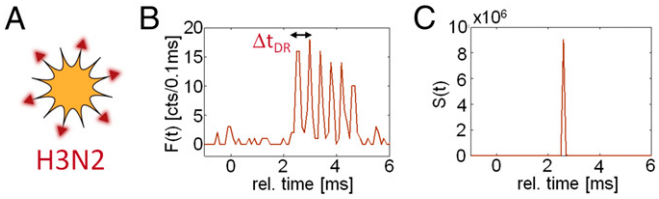

Fig. 3. Analysis of single-virus fluorescence signals. (*A*) Sketch of fluorescently labeled H3N2 virus, responding to excitation at 745 nm. (*B*) Fluorescence signal from single H3N2 virus showing six peaks with average spacing Δt_{DR}. (*C*) Corresponding processed signal using shift-multiply algorithm with Δt_{DR} showing dramatically increased SNR.

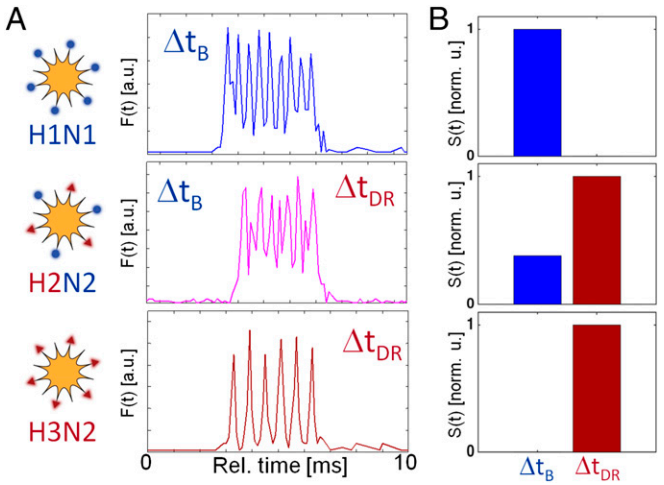

Fig. 4. Two-color combinatorial detection of single viruses. (*A*) Schematic view of labeling scheme for the three influenza types and their resulting single-virus fluorescence signals; the H2N2 virus shows a mixture of six and nine peaks upon blue and dark red excitation. (*B*) Bar histograms of signals after shift-multiply processing at Δt_B and Δt_{DR}. Singly labeled viruses appear in only one Δt channel, whereas the double-labeled virus creates signal in both color channels.

single-molecule detection sensitivity into the basis for a powerful and versatile diagnostic instrument for a variety of bioparticles and biomarkers. Beyond that, the ability to encode different wavelengths into unique spatial light patterns opens the door to new avenues for integrated photonic and optofluidic devices, for example spectrally reconfigurable optical particle traps or distribution of different colors to different areas on a chip.

Methods

Optofluidic ARROW Chip Fabrication and Waveguide Structure. The optofluidic chip used in this study was fabricated on a 100-mm silicon substrate on which a sequence of dielectric layers for optical guiding was sputter deposited. These cladding layers consisted of Ta_2O_5 and SiO_2 (refractive index, 2.107 and 1.46) chosen to minimize background photoluminescence (33). Their thicknesses in nm starting from the substrate were 265/102/265/102/265/102, where the material sequence reads $SiO_2/Ta_2O_5/SiO_2/Ta_2O_5/SiO_2/Ta_2O_5$. SU8 photoresist (SU8-10, MicroChem) was spun on the wafer, patterned, and developed to define the hollow waveguide channel with a rectangular cross-section 12 μm wide by 5 μm high. The SU8 and a thin nickel layer were used as a mask to etch a self-aligned pedestal into the wafer using an inductively coupled-plasma reactive ion etcher (ICP-RIE). The pedestal serves to raise the SU8 and subsequent hollow core above the wafer surface so it is surrounded by air on its sides. A single SiO_2 overcoat layer of 6-μm thickness was deposited over the SU8 by plasma-enhanced chemical vapor deposition. Three-μm-tall ridges were etched into the SiO_2 layer, again using the ICP-RIE, to form MMI and single-mode ridge waveguides that intersect multiple points of the hollow waveguide as illustrated in Fig. 1*B*. Fluid inlets into the hollow channel were exposed with a wet etch through the top SiO_2 layer and the SU8 was then removed with a H_2SO_4:H_2O_2 solution to form the hollow core. After rinsing and drying, the wafer was cleaved into individual chips of ~10 × 10 mm^2.

Virus Sample Preparation. Three inactivated, whole influenza virus samples were purchased for testing—β-Propiolactone-inactivated A/PR/8/34 (H1N1) and UV-inactivated A/2/Japan/305/57 (H2N2) (Advanced Biotechnologies Inc.) as well as Formalin-inactivated A/Aichi/68 (H3N2) (Charles River). Viruses were dyed using NHS-activated Dylight fluorophores according to manufacturer instructions (Thermo Scientific). Briefly, virus samples were added to aliquots of dried Dylight dyes and allowed to incubate at room temperature for 2 h. Samples were then separated from free dye using PD MiniTrap G-25 gel filtration columns (GE Healthcare). Fractions were collected dropwise and tested for fluorescent virus and free-dye background on a custom total internal reflection fluorescence (TIRF) microscope. Once identified, the viral fractions were aliquoted and flash-frozen via liquid nitrogen for later use. Although manufacturer concentrations were reported, the variable dilution/fractionation process of gel filtration chromatography leads to an inability to directly account for virus concentration. However, TIRF-based measurements concluded that virus concentrations were on the order of femtomolar as observed by direct counting on the chip.

Multiplex Virus Fluorescence Detection Setup and Experiment. A detection setup was used similar to that previously reported (19, 20, 30). The optical setup implements three lasers, a 488-nm Ar-ion laser, a 633-nm HeNe laser, and a Ti:sapphire laser tuned to 745 nm in continuous wave mode. All three of the laser lines were coupled into a single-mode fiber which then butt-coupled into a narrow (4-μm) single-mode-excitation solid-core waveguide on the ARROW optofluidic chip. The single-mode waveguide ends in the center of the 100-μm-wide and 3.4-mm-long MMI waveguide. In the MMI, multiple modes interfere with each other, creating equally separated spots at the liquid-core waveguide section. Fluorescently labeled viruses passing through the MMI excitation volume are subjected to the MMI pattern and thus produce multiple fluorescent signals per virus. These signals are captured by the liquid-core waveguide, transmitted into the collection solid-core waveguide, and are collected at the chip facet by an objective. The signal is collimated, passed through a single penta-bandpass optical filter (FF01-440/521/607/694/809–25, Semrock) to eliminate the excitation wavelengths, and is finally detected by a single-photon avalanche diode (Excelitas). No spectral filters to separate the emission colors are required.

ACKNOWLEDGMENTS. We thank M. Stone for providing access to a TIRF microscope for virus labeling characterization as well as R. A. Mathies, J. L. Patterson, and R. Carrion Jr. for stimulating discussions. We acknowledge support by the W. M. Keck Center for Nanoscale Optofluidics at University of California, Santa Cruz, the NIH under Grants 4R33AI100229 and 1R21AI100229, and the National Science Foundation (NSF) under Grants CBET-1159453 and CBET-1159423. Joshua W. Parks was supported by the Eugene Cota-Robles Fellowship and an NSF Graduate Research Fellowship under Grant DGE 0809125.

1. Brackett CA (1990) Dense wavelength division multiplexing networks: Principles and applications. *IEEE J Sel Area Commun* 8(6):948–964.
2. Siva Ram Murthy C, Guruswamy M (2001) *WDM Optical Networks, Concepts, Design, and Algorithms* (Prentice Hall, Upper Saddle River, NJ).
3. Agrawal GP (2010) *Fiber-Optic Communication Systems* (Wiley, New York).
4. Hood L, Heath JR, Phelps ME, Lin B (2004) Systems biology and new technologies enable predictive and preventative medicine. *Science* 306(5696):640–643.
5. Moerner WE, Kador L (1989) Optical detection and spectroscopy of single molecules in a solid. *Phys Rev Lett* 62(21):2535–2538.
6. Craighead H (2006) Future lab-on-a-chip technologies for interrogating individual molecules. *Nature* 442(7101):387–393.
7. Huang B, et al. (2007) Counting low-copy number proteins in a single cell. *Science* 315(5808):81–84.
8. Eid J, et al. (2009) Real-time DNA sequencing from single polymerase molecules. *Science* 323(5910):133–138.
9. He L, Özdemir SK, Zhu J, Kim W, Yang L (2011) Detecting single viruses and nanoparticles using whispering gallery microlasers. *Nat Nanotechnol* 6(7):428–432.
10. Zhao Y, et al. (2013) Lab-on-a-chip technologies for single-molecule studies. *Lab Chip* 13(12):2183–2198.
11. Zhao Y, et al. (2014) Dark-field illumination on zero-mode waveguide/microfluidic hybrid chip reveals T4 replisomal protein interactions. *Nano Lett* 14(4):1952–1960.
12. Johnson I, Spence MTZ, eds (2010) *Molecular Probes Handbook, A Guide to Fluorescent Probes and Labeling Technologies* (Molecular Probes, Eugene, OR), 11th Ed.
13. Martini J, et al. (2012) Time encoded multicolor fluorescence detection in a microfluidic flow cytometer. *Lab Chip* 12(23):5057–5062.
14. Cole RH, de Lange N, Gartner ZJ, Abate AR (2015) Compact and modular multicolour fluorescence detector for droplet microfluidics. *Lab Chip* 15(13):2754–2758.
15. Fan X, White IM (2011) Optofluidic microsystems for chemical and biological analysis. *Nat Photonics* 5(10):591–597.
16. Schmidt H, Hawkins AR (2011) The photonic integration of non-solid media using optofluidics. *Nat Photonics* 5:598–604.
17. Erickson D, Sinton D, Psaltis D (2011) Optofluidics for energy applications. *Nat Photonics* 5(10):583–590.
18. Soldano LB, Pennings ECM (1995) Optical multi-mode interference devices based on self-imaging: Principles and applications. *IEEE J Lightwave Technol* 13(4):615–627.
19. Liu S, et al. (2014) Correlated electrical and optical analysis of single nanoparticles and biomolecules on a nanopore-gated optofluidic chip. *Nano Lett* 14(8):4816–4820.
20. Liu S, et al. (2015) Electro-optical detection of single λ-DNA. *Chem Commun (Camb)* 51(11):2084–2087.
21. Schmidt H, Yin D, Barber JP, Hawkins AR (2005) Hollow-core waveguides and 2D waveguide arrays for integrated optics of gases and liquids. *IEEE J Sel Top Quantum Electron* 11(2):519–526.
22. Schmidt H, Hawkins AR (2008) Optofluidic waveguides: I. Concepts and implementations. *Microfluid Nanofluidics* 4(1-2):3–16.

23. Lien V, Zhao K, Berdichevsky Y, Lo Y (2005) High sensitivity cytometric detection using fluidic-photonic integrated circuits with array waveguides. *IEEE J Sel Top Quantum Electron* 11(4):827–834.
24. Rigler R, Elson ES (2001) *Fluorescence Correlation Spectroscopy: Theory and Applications* (Springer, Berlin).
25. Watzinger F, Ebner K, Lion T (2006) Detection and monitoring of virus infections by real-time PCR. *Mol Aspects Med* 27(2-3):254–298.
26. Ratcliff RM, Chang G, Kok T, Sloots TP (2007) Molecular diagnosis of medical viruses. *Curr Issues Mol Biol* 9(2):87–102.
27. Baccam P, Beauchemin C, Macken CA, Hayden FG, Perelson AS (2006) Kinetics of influenza A virus infection in humans. *J Virol* 80(15):7590–7599.
28. Suess T, et al. (2012) Comparison of shedding characteristics of seasonal influenza virus (sub)types and influenza A(H1N1)pdm09; Germany, 2007-2011. *PLoS One* 7(12): e51653.
29. Parks JW, et al. (2013) Hybrid optofluidic integration. *Lab Chip* 13(20):4118–4123.
30. Parks JW, et al. (2014) Integration of programmable microfluidics and on-chip fluorescence detection for biosensing applications. *Biomicrofluidics* 8(5):054111.
31. Testa G, Persichetti G, Sarro PM, Bernini R (2014) A hybrid silicon-PDMS optofluidic platform for sensing applications. *Biomed Opt Express* 5(2):417–426.
32. Testa G, Bernini R (2012) Integrated tunable liquid optical fiber. *Lab Chip* 12(19):3670–3672.
33. Zhao Y, et al. (2011) Hollow waveguides with low intrinsic photoluminescence fabricated with Ta_2O_5 and SiO_2 films. *Appl Phys Lett* 98(9):91104.